Effect of fluorination on the crystal and electronic structure of organometallic cyclopentadienyl-phenylenediamino-cobalt complexes

Effect of Fluorination on the Crystal and Electronic Structure of Organometallic Cyclopentadienyl-Phenylenediamino-Cobalt Complexes

Luca Pilia,[a,b,§*] Yoshiaki Shuku,[c] Simon Dalgleish,[c] Detlef W. M. Hofmann,[d] Nicola Melis,[a] Kunio Awaga[c] and Neil Robertson[b].

[a] Dipartimento di Ingegneria Meccanica Chimica e dei Materiali, Università di Cagliari, via Marengo 2, I09123, Cagliari, Italy.

[b] School of Chemistry and EaStChem, University of Edinburgh, King's Buildings, David Brewster Road, Edinburgh EH9 3FJ, UK.

[c] Department of Chemistry, Graduate School of Science, and Research Center of Materials Science Nagoya University, Chikusa-ku, Nagoya 464-8602, Japan.

[d] CRS4, Parco Scientifico e Tecnologico, Loc. Piscina Manna, I09010, Pula, Italy.

ABSTRACT

The fluorinated half sandwich complex [$CpCoL_F$] (Cp = cyclopentadiene; L_F = *o*-perfluoro-phenylenediimine; **2F**) shows a T-shaped geometry with the L_F ligand coplanar with the metallocycle. The molecules are dimerized in a head-to-tail fashion and arranged in a herringbone manner in the crystal packing. The crystal structure of **2F** is different from that of the corresponding hydrocarbon compound (**2H**). Moreover, the differences due to the presence of fluorine atoms are also highlighted by the analysis of the intermolecular contacts, which show that **2F** exhibits several F···F contacts, as well as aromatic intra-dimer π···π interactions in addition to C−H···π and C−H···F contacts. No relevant π···π interactions are observed in the case of **2H**. Hirshfeld Surface (HS) analysis also depicted well the differences in the solid state interactions between the different crystal structures. In particular, HS has been useful in highlighting the differences observed between the crystal structure of **2H** obtained from Rietveld refinement and that measured on single crystal (**$2H_P$** and **$2H_{SCH}$**, respectively). The effect of the fluorination on the electronic structure has been investigated also by CV measurements and Density Functional Theory calculations. Both are consistent with a lowering in energy of the molecular orbitals. Data Mining Force Field calculations clearly indicate that the **$2H_{SCH}$** structure is more stable than the **$2H_P$** one. These findings can be explained in terms of the energy of the intermolecular interactions. The enhanced stability of the fluorine substitute can be easily explained by the large number of strong interactions involving fluorine atoms.

Keywords: Cyclopentadienyl-cobalt complexes; fluorinated molecules; X-ray diffraction; DFT calculations; Force Field calculations.

INTRODUCTION

The remarkable interest in fluorinated compounds is related to their broad applications in several field such as materials, agrochemistry and the pharmaceutical industry.[1,2] The substitution of hydrogen atoms with fluorine atoms in a molecule strongly affects its chemical and physical properties. Compared to the corresponding hydrocarbon compounds, the fluorinated ones indeed, generally show enhanced thermal stability, viscosity and density, whereas surface tension, refractive index and dielectric constant are smaller, as are the boiling and melting points.[3] Furthermore, the fluorination also changes the solubility of the molecules towards higher hydrophobicity.[4,5]

Because of their electron-withdrawing capability, the presence of fluorine atoms lowers the energy levels of the molecular orbitals (MOs); in particular, the decrease in the energy of the highest occupied molecular orbital (HOMO) confers to the molecules higher stability versus degradative oxidation processes. Furthermore, the lowest unoccupied molecular orbital (LUMO) is stabilized as well; conferring to the molecule an acceptor capability which facilitates the electron injection process resulting, in some cases, in air-stable *n*-type or ambipolar semiconductors.[5-9]

The C−F bond is the strongest one in organic chemistry (≈ 450 kJ mol^{-1})[4] and is characterized by a large dipole moment due to the different electronegativity of the two atoms (2.5 *vs* 4.0 for C and F respectively, in the Pauling scale); this feature reduces the covalent character of the bond, increasing the electrostatic character.[1] Moreover, the low polarizability (α_D: 3.76 *vs* 4.5, for F and H respectively)[10] exhibited by the halogen atom results in a poor donor ability for fluorine. For these reasons, the intermolecular interactions shown by the C─F bond have mainly an electrostatic character. These interactions (in particular C─H···F─C) are of paramount importance in the supramolecular organization of these compounds and therefore heavily affect their solid state properties.[4,5,11,12]

Some of us have recently reported a detailed study on half sandwich cobalt complexes [CpCo(DAbnz)] (**2H**) and [CpCo(DAnap)] (**3H**) (Cp = cyclopentadiene; DAbzn = L_H = diaminobenzene; DAnap = diaminonaphthalene).[13] These compounds, which have been investigated for their potential (opto)electronic applications, present stable redox processes and two transitions in the visible and in the

near infrared (NIR) regions. Moreover, for both compounds, the intensities of the two absorptions are reversed in the solid state, with an enhancement of the absorption at lower energy and a suppression of that in the visible. This behavior has been attributed to the intermolecular interactions.

Taking into account the fluorination effects on the properties of a molecule, and in particular the fluorous effect-induced enhancement of the photo-stability[14] (which is very important for photo-detection applications) seemed interesting to us to investigate the structural and electronic effects induced by the substitution of hydrogen atoms with fluorine at the benzene ring of the complex **2H**. These effects are studied by single crystal X-ray diffraction measurements, UV-Vis-NIR spectroscopy, Density Functional Theory (DFT) and time-dependent DFT (TD-DFT) calculations and Hirshfeld surface analysis. Moreover, intermolecular interaction energy calculations, along with predictions of sublimation energies have been also performed by Force Field methods in order to investigate the effect of the fluorination on these properties.

Results and Discussion

SYNTHESIS AND CRYSTAL STRUCTURE – Complex **2F** was synthetized in good yield starting from **1F** and following the procedure previously reported by Richard F. Heck[15] (see Scheme 1) for the preparation of the corresponding hydrocarbon complex (**2H**).

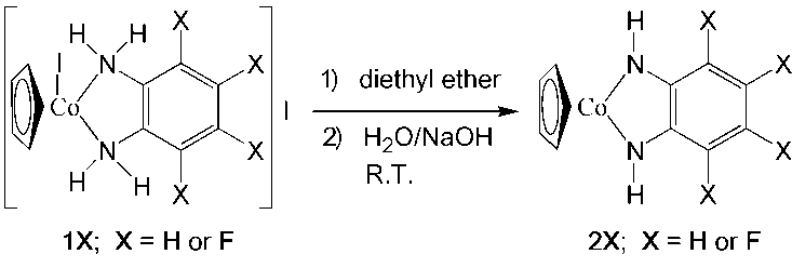

Scheme 1. Synthesis of complexes **2H** and **2F**.

Crystals of **2F** suitable for single crystal X-ray diffraction were obtained by evaporation of a diethyl ether solution; the crystallographic data are summarized in Table 1. The asymmetric unit, formed by four

molecules of the complex, two-by-two dimerized with a head-to-tail arrangement, is shown in Figure S1, whereas the structure of a single representative molecule is depicted in Figure 1 as an example.

Crystals of **2F** suitable for single crystal X-ray diffraction were obtained by evaporation of a diethyl ether solution; the crystallographic data are summarized in Table 1. The asymmetric unit, formed by four molecules of the complex, two-by-two dimerized with a head-to-tail arrangement, is shown in Figure S1, whereas the structure of a single representative molecule is depicted in Figure 1 as an example. Similar to the case of **2H**,[16] also the molecules of **2F** exhibits a T-shaped geometry with the cobalt ion in the same plane defined by the L_F moiety. The four molecules of the asymmetric unit of

Table 1. Crystallographic details for complex **2F**.

Formula	$C_{11}H_7CoF_4N_2$
Formula weight / g mol^{-1}	302.12
Temperature / K	123
Crystal dimensions / mm^3	0.06 × 0.06 ×0.04
System	Monoclinic
Space group	$P2_1/n$ (#14)
***a* /** Å	15.5537(5)
***b* /** Å	16.7136(5)
***c* /** Å	16.4218(6)
***β* /** °	100.520(18)
***V* /** Å^3	4197.1(2)
Z	16
ρ_{calcd} / g cm^{-3}	1.912
μ **(MoKα) /** cm^{-1}	16.726
***λ* /** Å	0.71075
$2\theta_{max}$ / °	54.9
Reflections collected	33268
Unique reflections (R_{int}**)**	9582 (0.0373)
Number of parameters	681
Final R_1 **[** $I > 2\sigma(I)$**]**	0.0419
wR_2 **(all data)**	0.0811
Goodness of fit	1.076
Residual electron density / Å^3	0.38 e$^-$

2F differ because of the different rotation of the cyclopentadienyl ring with respect to the plane containing the metal ion and the other ligand (see Figure S2).

This kind of distortion has been previously reported for other cyclopentadienyl metal complexes.[17] In the present case, considering that no significant differences can be predicted by DFT calculations (*vide infra*) in the energy of the orbitals and the molecules, these structural features are probably mainly due to solid state interactions rather than electronic reasons. The η^5-C_5H_5 (η^5-Cp) rings show an average dihedral angle of 88.22° with respect to the plane calculated on Co and L_F ligand; furthermore, the average of the distances between the metal ion and the centroid of the η^5-Cp ring is 1.652 Å. The C-N-Co-N-C cycles are planar (see Table S2) and are also almost coplanar with the corresponding phenylene rings (<av.> of dihedral angle = 1.41°). The bond distances are not unusual and with small differences among the four molecules (see Tables 2 and S1) with C−C, C−N and N−Co bond lengths ranging respectively, between 1.356−1.426, 1.344−1.352 and 1.837−1.851 Å.[18] Looking closer at the bond distances of the L_F moiety, the different C−C bond lengths at the benzene ring and the short C−N distances (π-character) suggest a *o*-benzoquinone nature for this ligand.[16,18] In addition, the Co-N-C bond angle amplitudes (115.89° <av.>) are in agreement with a sp^2 hybridization for the nitrogen atoms, and therefore consistent with this description of L_F ligand. The homologous hydrocarbon complex (**2H**) shows two molecules in the asymmetric unit arranged in a head-to-tail fashion.[19] Moreover, by inspecting bond distances and angles, conclusions similar to those reported above for L_F can be made also for the hydrocarbon ligand in **2H**. A *o*-benzoquinone character of the *o*-perfluoro-phenylenediimine moiety was found also for the complex (η^5-Cyclopentadienyl)-(*N*-perfluorophenyl-*o*-perfluoro-phenylenedi-imine)-cobalt (**3F**) which presents a perfluorophenyl group as substituent at one of the nitrogen atoms.[16,19] Therefore, accordingly with these findings and with previously reported studies on similar complexes,[20] also in the **2F** case, the most plausible oxidation state for the cobalt ion is +1.

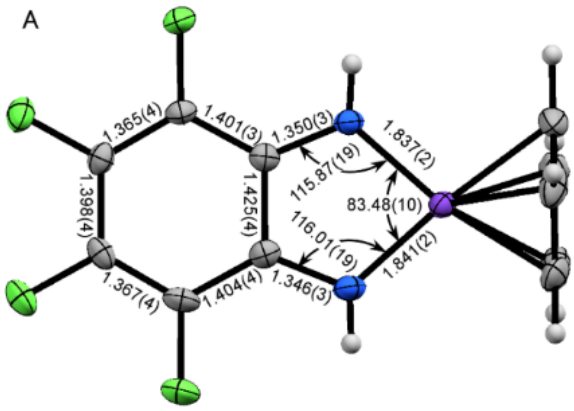

Figure 1. Molecular structure of one (A) of four crystallographically independent molecules with bond distances (Å) and angles (deg); thermal ellipsoids are at the 50% probability level.

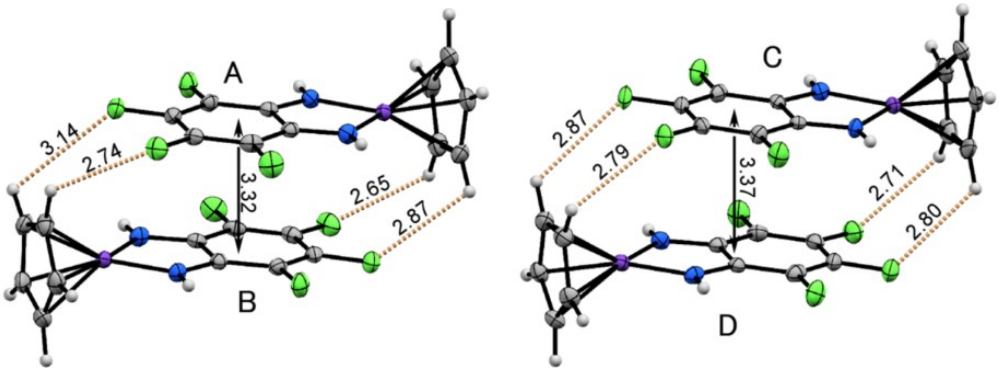

Figure 2. Crystal structures of two crystallographically independent dimers with intradimer short contacts (Å).

As far as the crystal packing is concerned, both **2H** and **2F** crystalize in the *P21/n* space group. However, the unit cell contains 8 and 16 molecules in the case of **2H** and **2F**, respectively. The packing motif of **2F** is formed from an alternation of two different type of dimers (Figure 2), arranged in a herringbone fashion (Figure S3). While the molecules of the dimers are almost parallel (angles between Co-L_F planes are smaller than 1°), the angles between the dimers are around 59° (see Figure S4). Furthermore, the angles between the plane of the Cp moieties are nearly parallel in a dimer (2.29 and

Table 2. Comparison between calculated and experimental selected bond distances (Å) and angles (deg) for **2F** in the case of molecule **C**.

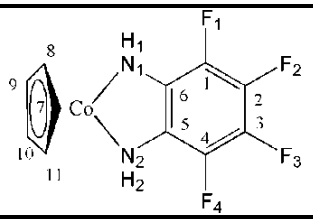

	B3LYP	BP86	Exp. (C)
Co-N1	1.850	1.851	1.840(2)
Co-N2	1.851	1.851	1.841(2)
C6-N1	1.349	1.355	1.348(3)
C5-N2	1.349	1.355	1.349(3)
C5-C6	1.427	1.438	1.423(3)
C1-C6	1.407	1.414	1.399(3)
C1-C2	1.376	1.386	1.363(4)
C2-C3	1.411	1.421	1.398(4)
C3-C4	1.376	1.386	1.360(4)
C4-C5	1.407	1.414	1.408(4)
C1-F1	1.351	1.360	1.357(3)
C2-F2	1.342	1.351	1.347(3)
C3-F3	1.342	1.351	1.346(3)
C4-F4	1.351	1.360	1.355(3)
Co-N1-C6	116.18	116.44	115.98(17)
Co-N2-C5	116.16	116.44	115.91(18)

1.83° for the A-B and C-D dimer, respectively) whereas those between dimers show an average value of 85.16° (Figure S5).

Many contacts shorter than the sum of the van der Waals (vdW) radii[21] are present between adjacent molecules in **2F** (see Table S4 and Figures 2, S3 and S6). In particular, those with a distance shorter than the sum of vdW radii by at least 0.20 Å mainly involve hydrogen atoms. Several F···F intermolecular contacts are also displayed by this complex, as well as aromatic intra-dimer π···π interactions (Figure 2). Moreover, several C−H···π and C−H···F contacts are present between dimers (Figures S3 and S4) conferring to the crystal packing the motif described above.[22] In the case of the corresponding hydrocarbon compound **2H**, the crystal structure obtained from Rietveld refinement of powder diffraction data (**2H$_P$**)[13] exhibits H···H intermolecular distances which seem too short to be realistic (1.88 and 1.92 Å; see Table S5). These contacts are shorter than 0.5 times of the sum of the VdW radii, likewise

two C···H interactions (2.308 and 2.529 Å). Despite a good agreement in the crystallographic parameters between this structure and that obtained from single crystal data (**2H$_{SC}$**)[16] some differences are present between the structures. In particular, the overlap of **2H$_{P}$** and **2H$_{SC}$** highlights a different conformational rotation of the cyclopentadienyl rings (Figure S7).

With the aim of shedding light on the short H···H contacts, and since the crystal structure obtained from single crystal[16] (ref CAFJEY) do not report hydrogen atoms, we added them with *Mercury*[23] and refined the structure (**2H$_{SCH}$**). The shortest contacts observed in this structure are between the hydrogen at the nitrogen atoms and carbon atoms of the L_H ligand (2.611 Å). The distance is 0.2 time below the sum of vdW radii, which coincides with the expectations. The differences in the intermolecular contacts between the two structures are mainly related to the different conformational rotation of the cyclopentadienyl rings.

ELECTROCHEMISTRY AND ELECTRONIC SPECTROSCOPY – The redox properties of **2F** were investigated in CH_3CN solution through cyclic voltammetry measurements as described in the Experimental part. As one can see in Figure 3, similarly to **2H**, also **2F** shows two reversible redox processes: a reduction (from **2F** to **2F^{-1}**) with a half-wave potential of −1.52 V (*vs* Fc/Fc^+) and an oxidation at 0.13 V (from **2F** to **2F^{+1}**). As expected, and in accordance with DFT calculations, the presence of fluorine atoms makes the complex **2F** more difficult to be oxidized and easier to be reduced, in comparison to **2H**. Indeed, in the case of **2H**, the same redox processes fall at −1.83 and −0.13 V, respectively.

From the electrochemical data the HOMO energy was estimated following the method proposed by D'Andrade *et al.*[24] giving a value of −4.78 eV, in good agreement with the calculated one (−4.88 eV in CH_3CN). Moreover, the HOMO-LUMO energy gap roughly evaluated[25] from the difference between the onset of the redox processes is ≈1.48 eV in accordance with the DFT calculations (1.41 and 1.42 eV for gas-phase and CH_3CN, respectively).

The electronic spectrum of **2F** measured in CH_3CN solution is reported in Figure 4. A strong absorption (ε = 1.577×10^4 dm^3×mol^{-1}×cm^{-1}) is present in the visible region (532 nm), along with a weak one (ε = 590 dm^3×mol^{-1}×cm^{-1}) in the NIR at 720 nm. These transitions have been mainly assigned by TD-DFT calculations to HOMO−2→LUMO and HOMO→LUMO, respectively (see below). These features are very similar to those shown by **2H** (λ_{max} = 523 and 740 nm). In addition, the absorption in the NIR region exhibits a small solvatochromic effect (Figure S10) in agreement with the reduced charge transfer (CT) character associated to this transition (*vide infra*). Moreover, analogously to what was found in the case of **2H**, a dramatic increase of the NIR absorption intensity in the solid state is observed also for the fluorinated complex (Figure 4). Indeed, the intensity ratios I_{Vis}/I_{NIR} are 26.7 and 1.4 in solution and in the solid state, respectively. Furthermore, small shifts of the peaks positions have been observed in the case of **2F** (542 and 726 nm). The HOMO-LUMO gap estimated from the onset of the NIR absorption gives a value of 1.46 eV, in good agreement with the DFT value and that obtained from the electrochemical measurements.

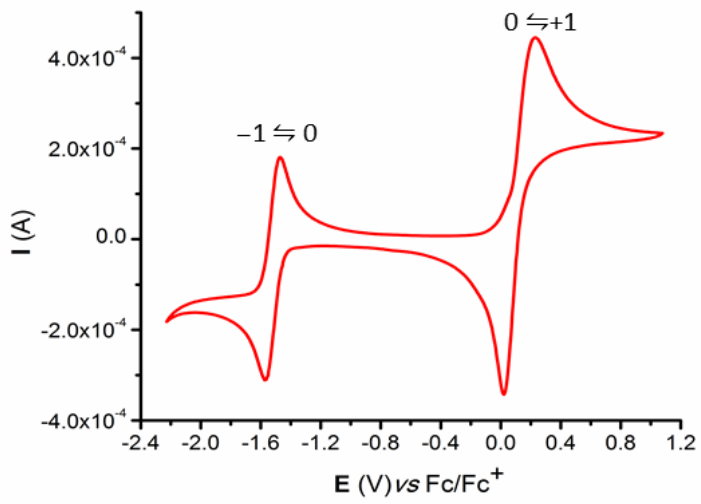

Figure 3. Cyclic voltammogram of **2F** in CH_3CN degassed solution at a scan rate of 0.100 V/s.

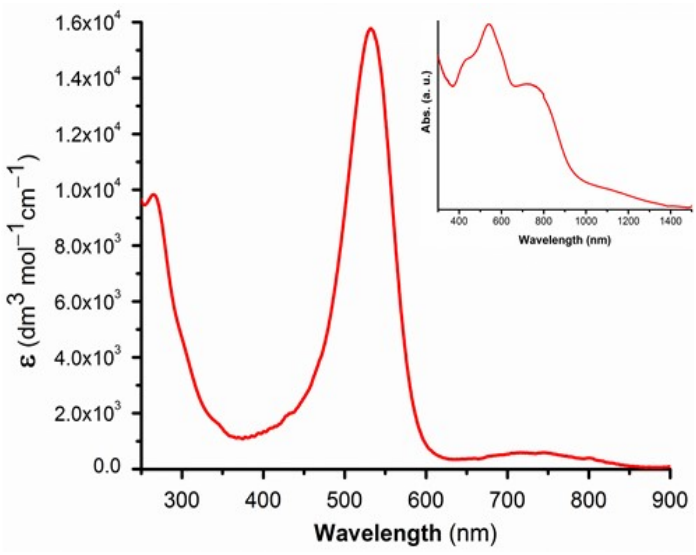

Figure 4. UV-vis-NIR spectrum of **2F** complex in CH_3CN solution. The inset shows the diffuse reflectance spectrum.

DFT CALCULATIONS - DFT calculations at the BP86/ and B3LYP[26]/ triple-zeta 6-311+G(d,p) level of theory have been performed on both **2H** and **2F** complexes to investigate the effect of fluorination at the phenyl ring on the electronic structure of **2F**. The geometries were optimized starting from the X-ray structures (see Figure S11); calculated bond distances and angles result in very good agreement with the crystallographic data (Tables 2 and S6) with the largest discrepancies of 0.026 Å and 0.53° for distances (C3—C4 bond) and angles (Co-N2-C5), respectively, in the case of BP86 functional. Even though the general shape of the MOs and their energetic sequences are very similar (except for the reversal of HOMO—3 and HOMO—4; Table S7) the MOs of **2F** are generally lower in energy by about 0.5-0.6 eV in comparison with those of the corresponding orbitals of **2H** (Table S8 and Figures S12 and S13), in accordance with the electronic effect of fluorine atoms. As far as the frontier orbitals (FOs) are concerned, they are delocalized all over the molecule, with contributions from the orbitals of all the parts of the complex (see Table S9). In particular, the HOMO is formed with contributions of 38, 15 and 46% from L_F, Cp and Co, respectively; whereas the corresponding values in the case of the LUMO are 33, 40 and 27 %.

Calculations with the same basis-set but using B3LYP as the functional, have also been performed. Although, on the whole, the geometric parameters are similar to those predicted with B3LYP, with

distances slightly shorter by about 0.01 Å, the energy of the orbitals are significantly different and some inversions in the order of the orbitals are also found (Table S7 and S8 and Figures S12 and S13). For instance, the energy of the HOMO is −5.70 eV *vs* −4.93 eV predicted by BP86, whereas that of LUMO orbital is −2.89 eV (E_{LUMO}(BP86) = −3.52 eV). Taking into account the experimental results (see cyclic voltammetry and UV-Vis data), it seems that the HOMO and LUMO levels, as well as their energy gap, are significantly better predicted by BP86 rather than B3LYP. Moreover, the HOMO calculated with BP86 corresponds to the HOMO-1 predicted with B3LYP, and vice versa. Similar considerations can be done for the DFT calculations concerning the **2H** complex.

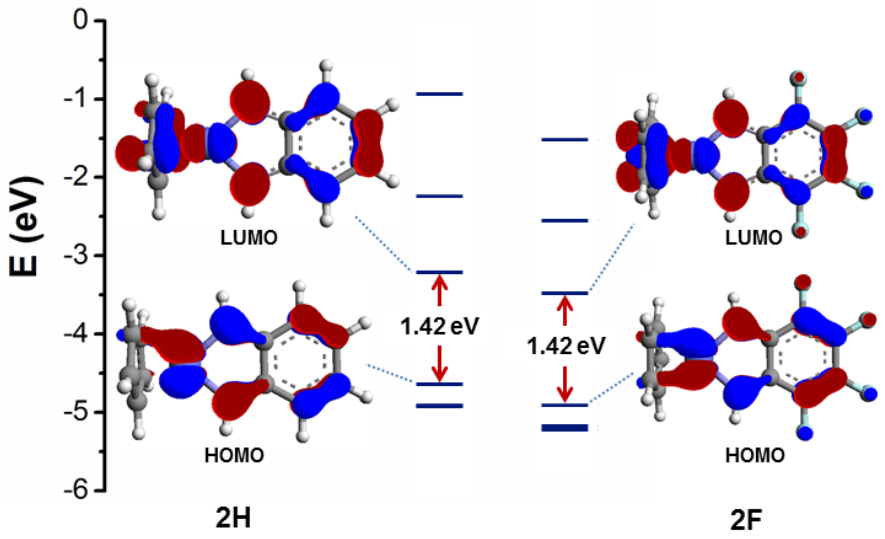

Figure 5. Frontier Orbitals of **2H** and **2F** calculated by DFT methods in CH_3CN at BP86/6-311+G(d,p) level of theory (contour value of 0.040).

The electronic absorption spectrum of **2F** in CH_3CN was simulated by TD-DFT calculations with the Polarizable Continuum Model employing both B3LYP and BP86 functionals. The results are reported in Figures S14-S17 and summarized in Table S10. The experimental measurement is better reproduced by calculations in the case of BP86 functional (λ_{max} = 464 and 735 nm) rather than with the B3LYP (λ_{max} = 466 and 922 nm); in particular for the position of the transition in the NIR region and for the ratio between the intensities (and oscillator strengths) of this absorption and that in the visible region.

Moreover, differences in the findings obtained with the two functionals are also observed in the orbitals contributions to the transitions (see Table S10). Indeed, the NIR absorption is a HOMO□ LUMO transitions and HOMO−1→LUMO for BP86 and B3LYP, respectively.

The effect due to the fluorination on electron density distribution on the complex is well highlighted also by the electrostatic potential (EP) mapped on the density surface shown in Figure S18. In **2H** the part of the molecule showing negative EP is mainly localized on the nitrogen and carbon atoms of L_H (electron-rich aromatic system) and, to a lesser extent, on those of Cp ligand; whereas it is positive on the hydrogen atoms. Instead, in the case of **2F** the most negative EP is located on the fluorine atoms, while it is only slightly negative at the phenylene ring. The reason for this is related to the polarization effect of the halogen atoms which draw the electronic density away from the aromatic core. These findings may explain the different π···π interactions observed in the two complexes. Indeed, the relatively large negative charge on the benzene ring in **2H** may hamper the overlap between the benzene moieties in **2H** because of the electrostatic repulsions. In the case of **2F** instead, the EP is almost neutral and this allows a good overlap between the aromatic rings.[22] Moreover, the polarization effect due to the presence of fluorine atoms is also confirmed by the calculated molecular dipole moment which increases from 1.49 to 5.50 D going from **2H** to **2F**. No important differences concerning the EP have been found between the results predicted by the two different functionals used for DFT calculations.

HIRSHFELD SURFACE ANALYSIS – With the aim of studying the difference in the solid-state interactions between the **2H** and **2F** complexes, Hirshfeld surface (HS)[27-29] analyses have been performed. In Figures 6, S19 and S20 are depicted the HSs of the two compounds mapped with the normalized contact distances (d_{norm}).[28] The HS color code indicates by blue, white and red spots, distances which are respectively, longer, equal or shorter than the sum of vdW radii (for more details on d_{norm} see the SI). As one can see, the $\mathbf{2H_P}$ HS shows more numerous and more extended red spots, suggesting stronger intermolecular contacts in comparison with **2F** and $\mathbf{2H_{SCH}}$, in accordance with the X-ray findings. However, as reported above, the crystal structure obtained from powder data shows too short H···H

contacts due to the rotation of the cyclopentadienyl ring, and this heavily affects the HS appearance (see below). Both **2F** and **2H$_{SCH}$** exhibit red spots in correspondence with hydrogen atoms of the N−H groups, confirming the role played by these atoms in the intermolecular contacts. In addition, the HS of **2F** presents also red spots due to the interactions related to F2 and F3 atoms (see the structural formula reported in Table 2).

The Hirshfeld fingerprint plots (FPs),[30,31] which give an overall two-dimensional depiction of the intermolecular contacts occurring in the crystal, help to highlight the expected differences in the interaction types in the two complexes (see Figures 6, S21-S23). The FP of **2F** presents (Figure 6c) in the bottom left region of the plot the fingerprint relative to F···H (and H···F), N···H, H···C and F···F contacts. The **2H$_{P}$** FP exhibits three sharp peaks in the same region, related to short H···H, C···H (and H···C) and N···H interactions, whereas **2H$_{SCH}$** shows rounded peaks and at longer distance corresponding to the same kind of intermolecular interactions. Therefore, the FP analysis clearly highlights the differences in the two crystal structures reported for complex **2H**. Moreover, in agreement with the different features of the structures, the FPs of the two complexes display remarkable dissimilarities in the region related to the π···π interactions, as clearly shown by the different colors presented in that part (bins corresponding to d_e and $d_i \approx 1.8-2.0$ Å). Indeed, the color of a bin depends on the fraction of total points of the HS belonging to that bin. The color can change from blue, for the smallest contributions, to red for contributions ≥ 0.1% of the surface.[30] Moreover, by fingerprint analysis it is possible to assess the contributions from the different intermolecular contacts to the HS. In Figures S24-S29 are reported the percentage contributions to the HS for the complexes **2F** and **2H**, respectively. Whereas in the hydrocarbon compound, more than three quarters (76 and 77% for **2H$_{P}$** and **2H$_{SCH}$**, respectively) of the contribution is related to H···X contacts (X = H, N and C) with the largest percentage due to H···H (between 57 and 63%), in the **2F** case, the fluorine atoms are involved in roughly 50% of contributions to the HS (F···X; X = F, C, H). Furthermore, in accordance with the absence of π···π interactions in **2H**, no contributions from C···C contacts have

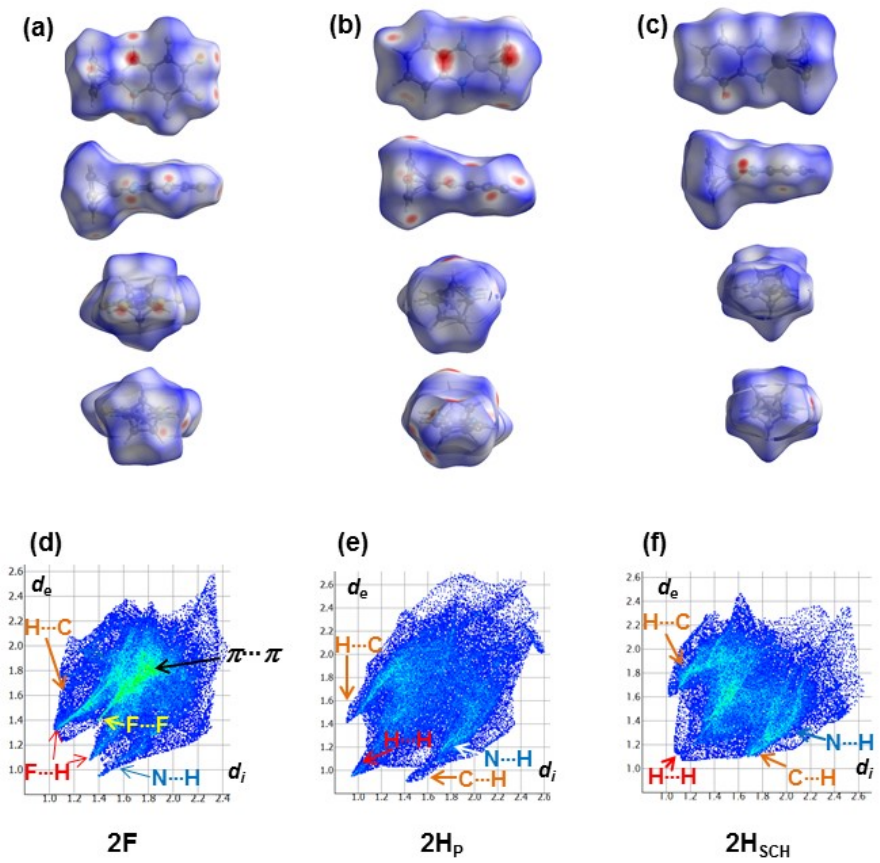

Figure 6. Hirshfeld surfaces for 2F (a), $2H_P$ (b; P = powder) and $2H_{SCH}$ (c; SCH = single crystal with added hydrogen atoms) and the corresponding fingerprint plots (d, e and f).

been found. The dissimilarities in the aspect of both HSs and FPs, especially in the case of **$2H_P$** and **$2H_{SCH}$**, confirm the capability of these analyses to highlight differences between crystal structures which look apparently very similar.

ANALYSIS OF THE STRUCTURES WITH FORCE FIELD CALCULATIONS – Force Field calculations allow one to analyze the interactions of the molecules in terms of atom pairs on an energetic level. This force field is strictly based on atom pair interactions under the assumption that the total interaction energy E_{IJ} between two molecules I and J can be written as sum of pair interactions. For our calculations we used the program *FlexCryst*.[32] This program is parameterized for all atoms including cobalt. The Force Field has been parameterized by data mining on existing crystal structures and is named for this reason as data mining force field (DMFF). For more details, the reader might refer to the Supplementary Information

and references 33 and 34. The crystal structures have been taken from this work in the case of **2F**, from reference 13 for $\mathbf{2H_P}$, and from *Mercury* for $\mathbf{2H_{SCH}}$ (reference code CAFJEY). The missing hydrogen atoms have been added with the auto-editing tool of *Mercury*.[23]

In a first step we tested the DMFF for the structures by structure minimization. If the crystal structure is correct, the structure should change by very little upon minimization. Two common measurements for the similarity before and after minimization are the densities and the energies. The change in the density is for two structures below 1% and only for the structure $\mathbf{2H_P}$ it is as high as 7%. A similar picture was obtained for the energies. The change in the energy is for two cases (**2F** and $\mathbf{2H_{SCH}}$) was below 20%, and only above for structure $\mathbf{2H_P}$ (see Table 3). The figures with plotted pair interactions give further insight. In Figure 7 the five strongest stabilizing (green) and destabilizing (red) interactions are plotted for two molecules within the crystal (see also Table S11).

The crystal structure of $\mathbf{2H_{SCH}}$ coincides quite well with the expectations. The main interaction involves the hydrogen atom at the NH group. In addition, we find some interactions with the cobalt and carbon. In contrast, the structure of $\mathbf{2H_P}$ shows, in addition, a very destabilizing interaction between hydrogen atoms (9.2 kJ mol^{-1}). This interaction is caused by the slight rotation of the cyclopentadienyl (Figure S7). As a consequence, the total energy rises from −76 kJ mol^{-1} to −62 kJ mol^{-1}, and the result favors clearly the structure $\mathbf{2H_{SCH}}$ as more stable. The small inaccuracies, which are connected with structure determination from powder diagrams, are large enough to be recognized by the force field. The fluorine substitute, **2F**, shows a huge number of additional interactions, which are formed with the fluorine atoms. The strong binding interactions are able to compensate the occurring destabilizing interactions. The lattice energy lowers from −76 to −242 kJ mol^{-1}.

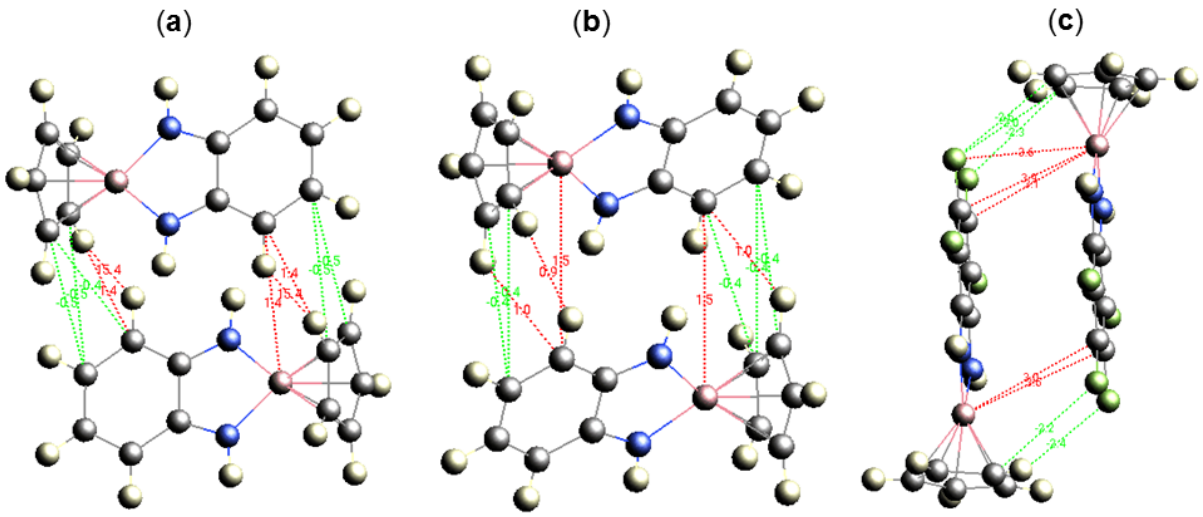

Figure 7. DMFF calculated pair interactions for **2H$_P$** (a), **2H$_{SCH}$** (b) and **2F** (c). The attractive and repulsive interactions are reported in green and red, respectively.

Table 3. Energy calculations with a force field.

	2F	**2H$_P$**	**2H$_{SCH}$**
Lattice Energy exp. *(kJ mol^{-1})*	-242	-62	-76
Lattice Energy minimized *(kJ mol^{-1})*	-270	-76	-80
Delta G *(%)*	12	21	5
Density exp. *(g cm^{-3})*	1.91	1.56	1.56
Density minimized *(g cm^{-3})*	1.92	1.44	1.56
Delta d *(%)*	0.81	-7.44	0.21

CONCLUSIONS

The fluorinated Co half sandwich complex **2F** shows a T-shaped geometry with the L$_F$ (*o*-perfluoro-phenylenediamine) ligand coplanar with the metallocycle. The molecules are dimerized in a head-to-tail fashion and arranged in a herringbone manner in the crystal packing. The crystal structure of **2F** is different from those of the corresponding hydrocarbon compound. Moreover, the differences induced by the presence of fluorine atoms are also highlighted by the analysis of the intermolecular contacts

which show that **2F** exhibits several F···F contacts, as well as aromatic intra-dimer π···π interactions, in addition to C−H···π and C−H···F contacts which are present between dimers. No relevant π···π interactions are present in **2H**. Hirshfeld surface analysis also depicted well the differences in the solid state interactions between the different crystal structures. In particular, this analysis has been successful in highlighting the differences observed between the crystal structure of **2H** obtained from Rietveld refinement of powder diffraction data and that measured on single crystal (**2H$_P$** and **2H$_{SCH}$**, respectively).

The effect of fluorination on the electronic structure has been investigated also by CV measurements and DFT calculations. Both are consistent with a lowering in energy of the molecular orbitals; the effect is almost the same for all the orbitals, in agreement with the similarity observed between the electronic spectra of **2F** and **2H**.

Data mining force field calculation clearly indicate the crystal structure **2H$_{SCH}$** is more stable than **2H$_P$**. These findings can be explained in terms of the energy of the intermolecular interactions. The enhanced stability of the fluorine substitute can be easily explained by the large number of strong interactions with fluorine.

EXPERIMENTAL SECTION

All the reagents and solvents were purchased from Aldrich and used without further purification. The complex $CpCoI_2CO$ and the ligand 3,4,5,6-tetrafluoro-1,2-phenylenediamine ($C_6F_4(NH_2)_2$, HL_F) were prepared as previously described in references 35 and 36, respectively.

Preparation

[CpCoI(L_FH_2)]I (**1F**)**.** *Synthesis*: complex **1F** was prepared by modifying the procedure reported by Richard F. Heck[15] for the corresponding compound with L_HH_2. 1.265 g (3.12 mmol) of $CpCoI_2CO$ in 10 mL of CH_2Cl_2 was added to 600 mg (3.12 mmol) of $C_6F_4(NH_2)_2$ in 5 mL of the same solvent and stirred at room temperature for 1.5 h. The formed solid was collected by filtration, washed with CH_2Cl_2 and dried (890 mg). After a partial evaporation of the mother liquid, a further 900 mg of product was obtained and combined

with the first crop. Total yield 1.590 g, 2.85 mmol (91%). Analytical results are in accordance with the formula [$CpCoC_6F_4(NH_2)_2I_2$]. *Elemental Analysis*: calculated for $C_{11}H_9CoF_4I_2N_2$ (557.94): C 23.68, H 1.63, N 5.02; found: C 23.49, H 1.58, N 5.00.

[CpCo(L_F)] (**2F**)**.** *Synthesis*: complex **2F** was prepared modifying the procedure reported in reference 15. 800 mg (1.43 mmol) of **1F** in 80 mL of diethyl ether and 5 mL of an aqueous solution of NaOH (115 mg in 5 mL), were shaken in a separatory funnel for ten minutes. Then the aqueous phase was removed and another 5 mL portion of the NaOH solution was added and the resulting mixture shaken for a further ten minutes. After removed the aqueous phase, the ether solution was washed twice with water and dried with Na_2SO_4. After filtration, the solvent was removed by evaporation at reduce pressure leading to a greenish crystalline solid. Yield 410 mg, 1.36 mmol; 95%). Analytical results are in accordance with the formula [$CpCoC_6F_4(NH)_2$]. *Elemental Analysis*: calculated for $C_{11}H_7CoF_4N_2$ (302.11): C 43.73, H 2.34, N 9.27; found: C 43.40, H 2.38, N 8.93. UV-Vis-NIR [in CH_3CN; λ, nm (ε, $dm^3 \times mol^{-1} \times cm^{-1}$)]: 724 ($5.87 \times 10^2$); 532 ($1.577 \times 10^4$); 431 (sh); 343 (sh); 267 (9.83×10^3). *FT–IR*: ν_{max}/cm^{-1} 3387 (m), 3313 (m), 1639 (w), 1506 (s), 1494 (s), 1416 (m), 1367 (s), 1333 (s), 1247 (s), 1109 (w), 1054 (ms), 1003 (s), 974 (vs), 832 (s), 819 (m), 801 (m), 692 (s), 672 (s), 661 (s), 643 (m), 634 (ms), 601 (vs), 578 (ms), 417 (vs).

Elemental Analyses were performed with a Carlo Erba CE1108 Elemental Analyser. Electronic absorption spectra were recorded with an Agilent Cary 5000 spectrophotometer equipped with a diffuse reflectance accessory - solution measurements (CH_3CN) were recorded using a quartz cell of path length 1 cm, while diffuse reflection measurements were run on KBr pellets. Fourier Transform infrared (FT-IR) spectra in the Mid-IR range (4000-400 cm^{-1}) were recorded on a Bruker Tensor 27 spectrometer equipped with a Platinum-ATR accessory and a DTGS (deuterated triglycine sulfate) detector. Cyclic voltammograms were carried out using an μAUTOLAB Type III potentiostat, driven by the GPES electrochemical software; employing a conventional three-electrode cell consisting of a platinum wire working electrode, a platinum wire as counter-electrode and Ag/AgCl in a 3.0 $mol \cdot dm^{-3}$ KCl solution as reference electrode. The experiments were performed at room temperature (25°C), in dry and degassed CH_3CN containing 0.1 mol dm^{-3} Bu_4NPF_6 as

supporting electrolyte, at 25-200 mV s^{-1} scan rate. Data are quoted against the ferrocene/ferrocenium couple (internal standard); under the above conditions the half-wave potentials for F_c/F_c^+ is +0.426 V vs. Ag/AgCl.

X-ray measurements

Single crystals of **2F** suitable for X-ray diffraction were grown by evaporation of a diethyl ether solution. Data were acquired with Mo-Kα radiation (λ = 0.71075 Å) on a Rigaku AFC10 Saturn-70 CCD diffractometer at 123 K. Data collection, cell refinement and data reduction were carried out using *CrystalClear* software.[37] The structure was solved by direct methods,[38] giving the positions of all nonhydrogen atoms, and refined using SHELX[38] software and the *CrystalStructure* (version 4.2.5) structure visualizer[39] using a full-matrix least-squares refinement procedure on F^2, with nonhydrogen atoms refined anisotropically, and hydrogen atoms placed at calculated positions. Details of the crystallographic data are given in Table 1. CCDC 1970222 contains the supplementary crystallographic data for complex **2F**.

DFT calculations

Ground-state electronic structure calculations of **2F** and **2H** were performed at DFT[40] level employing the GAUSSIAN 09[41] software package. The functionals used throughout this study were B3LYP[26] and BP86.[42] The ground state geometries were obtained in the gas phase by full geometry optimization without any symmetry constraints. The basis set employed for all atoms was the valence triple-zeta 6-311+G(d,p).[43] All structures were input starting from the crystallographic data. The atomic orbital compositions were calculated using a Simple Contribution Analysis. The effects of solvation on the complexes were taken into account using the Polarizable Continuum Model (PCM); the ground state geometry was optimized in a CH_3CN simulated electric field. The 10 lowest singlet excited states of the closed shell complexes were calculated within the TD-DFT formalism as implemented in Gaussian,[44] both, in the gas phase and in CH_3CN. The optimized molecular structures and the orbital isosurfaces were visualized using ArgusLab 4.0.[45]

Hirshfeld surface analysis

The Hirshfeld surface (HS) analysis[27] was performed as reported in reference 46 and further described in the SI; all the calculations on the HS surface and its properties were performed by the *CrystalExplorer* 3.1 program.[47]

Force Field calculations

Force Field calculations were performed using the program *FlexCryst*.[32] The Force Field has been parameterized by data mining on existing crystals. For details, the reader might refer to the references.[33,34] The crystal structures have been taken from this work for **2F**, from reference 13 for **2H$_P$**, and from *Mercury*[23] for **2H$_{SC}$** (reference code CAFJEY). The missing hydrogen atoms were added employing *Mercury* using the module auto edit. For further calculations, the obtained structure has been used.

ASSOCIATED CONTENT

Supporting Information

Additional figures of structures; tables with selected bond distances and angles, both experimental and calculated; tables with short intermolecular contacts; absorption spectra of **2F**; optimized geometry of **2F**; molecular orbitals of **2F** and **2H**; Tables with calculated atomic percentage contributions to some orbitals and assignment of electronic absorption spectra; TD-DFT calculated electronic spectra; Hirshfeld surface analysis; table with DMFF calculated strongest intermolecular interactions.

Present Address

§Dipartimento di Ingegneria Meccanica Chimica e dei Materiali, Università di Cagliari, via Marengo 2, I09123, Cagliari, Italy.

Conflict of interest

The authors declare that they have no conflict of interest.

Abbreviations

2F, [$CpCoL_F$]; **2H**, [$CpCoL_H$]; Cp, cyclopentadiene; DAbzn = L_H = diaminobenzene; DFT, density functional theory; DMFF, data mining force field; EP, electrostatic potential; HOMO, highest occupied molecular orbital; HS, Hirshfeld surface; L_F, *o*-perfluoro-phenylenediimine; LUMO, lowest unoccupied molecular orbital; PCM, polarizable continuum model; TD-DFT, time-dependent DFT; vdW, van der Waals.

ACKNOWLEDGEMENTS

L. P. thanks the FP-7 PEOPLE-Marie Curie Research Program IEF (contract number: PIEF-GA-2009-252273). L. P. and N. M. acknowledge the Fondazione di Sardegna, Project: "Precious metal-free complexes for catalytic CO_2 reduction" (CUP: F71I17000170002) for the financial support. Dr Francesca Mocci is kindly acknowledged for providing the computing facility.

REFERENCES

1. O'Hagan, D. Understanding organofluorine chemistry. An introduction to the C–F bond. Chem. Soc. Rev., **2008**, *37*, 308–319.

2. Kirsch, P. Modern Fluoroorganic Chemistry: Synthesis, Reactivity, Applications, Wiley-VCH, Weinheim, **2004**.

3. Siegemund, G.; Schwertfeger, W.; Feiring, A.; Smart, B.; Behr, F.; Vogel, H.; McKusick, B. and Kirsch, P. *Fluorine Compounds, Organic.* in Ullmann's encyclopedia of industrial chemistry. Wiley-VCH Verlag GmbH & Co. Hoboken, NJ, **2016**.

4. Pagliaro, M.; Ciriminna, R. New fluorinated functional materials. *J. Mater. Chem.*, **2005**, *15*, 4981–4991.

5. Babudri, F.; Farinola, G. M.; Naso, F.; Ragni, R. Fluorinated organic materials for electronic and optoelectronic applications: the role of the fluorine atom. *Chem. Commun.* **2007**, 1003-1022.

6. Brinkmann, H.; Kelting, C.; Makarov, S.; Tsaryova, O.; Schnurpfeil, G.; Wöhrle, D.; Schlettwein, D. Fluorinated phthalocyanines as molecular semiconductor thin films. *Phys. Stat. Sol. (a)* **2008**, *205*, 409–420 and references therein.

7. de Oteyza, D. G.; El-Sayed, A.; Garcia-Lastra, J. M.; Goiri, E.; Krauss, T. N.; Turak, A.; Barrena, E.; Dosch, H.; Zegenhagen, J.; Rubio, A.; Wakayama, Y.; Ortega, J. E. Copper-phthalocyanine based metal–organic interfaces: The effect of fluorination, the substrate, and its symmetry. *J. Chem. Phys.* **2010**, *133*, 214703-1–3.

8. Cardia, R.; Malloci, G.; Bosin, A.; Serra, G.; Cappellini, G. Computational investigation of the effects of perfluorination on the charge-transport properties of polyaromatic hydrocarbons. *Chem. Phys.* **2016**, *478*, 8–13.

9. Pilia, L.; Matsushita, M.M.; Awaga, K.; Robertson, N. Fluorination induced electronic effects on a Pt(II) square-planar complex of the: *O*-phenyenediimine ligand. *New J. Chem.* **2017**, 41, 5487–5492.

10. Schwerdtfeger, P. at http://ctcp.massey.ac.nz/dipole-polarizabilities.

11. Berger, R.; Resnati, G.; Metrangolo, P.; Weber, E.; Hulliger, J. Organic fluorine compounds: a great opportunity for enhanced materials properties. *Chem. Soc. Rev.* **2011**, *40*, 3496–3508.

12. Reichenbächer, K.; Süss, H. I.; Hulliger, J. Fluorine in crystal engineering "the little atom that could". Chem. Soc. Rev. **2005**, 35, 22–30.

13. Reinhardt, M.; Dalgleish, S.; Shuku, Y.; Reissig, L.; Matsushita, M. M.; Crain, J.; Awaga, K.; Robertson, N. Molecular and thin film properties of cobalt half-sandwich compounds for optoelectronic application. *Phys. Chem. Chem. Phys.* **2017**, 19, 6768–6776.

14. (a) Zhang, Z.; Xiong, J.; He, G.; Dang, D.; Xiea, Y.; Wang, Q. Fluorous effect-induced emission of azidosubstituted poly(vinylidenefluoride) withhigh photostability and film formation. *Polym. Chem.* **2020**, DOI: 10.1039/c9py01622h; (b) Sun, H.; Putta, A.; Kloster, J. P.; Tottempudi, U. K. Unexpected photostability improvement of aromatics in polyfluorinated solvents. *Chem. Commun.*, **2012**, 48, 12085–12087; (c) Renikuntla, R.; Rose, H. C.; Eldo, J.; Waggoner, A. S.; Armitage, B. A. Improved Photostability and Fluorescence Properties throughPolyfluorination of a Cyanine Dye. *Babu. Org. Lett.* **2004**, 6, 909–912.

15. Heck, R. F. Cyclopentadienylcobalt Derivatives of Chelating Aromatic Ligands. *Inorg. Chem.* **1968**, *8*, 1513–1516.

16. Rheingold, A. L.; Fultz, W. C.; Brill, T. B.; Landon, S. J. Crystal and molecular structure of (η^5-C_5H_5)Co(HNC_6H_4NH), a cobalt *o*-quinonediimine complex. J. Crystallogr. Spectrosc. Res. **1983**, *13*, 317–323.

17. Holland, P. L.; Smith, M. E.; Andersen, R. A.; Bergman, R. G. X-ray Crystal Structures of Cp*Ni(PEt_3)X [X = Br, O(*p*-C_6H_4Me), NH(*p*-C_6H_4Me), S(*p*-C_6H_4Me), OCH_3, $CH_2C_6H_5$, Me, H, PEt_3+]. Understanding Distortions and Trans Influences in Cyclopentadienyl Complexes. *J. Am. Chem. Soc.* **1997,** *119,* 12815–12823; and references therein.

18. Bill, E.; Bothe, E.; Chaudhuri, P.; Chlopek, K.; Herebian, D.; Kokatam, S.; Ray, K.; Weyhermüller, T.; Neese, F.; Wieghardt, K. Molecular and Electronic Structure of Four- and Five-Coordinate Cobalt Complexes Containing Two *o*-Phenylenediamine- or Two *o*-Aminophenol-Type Ligands at Various Oxidation Levels: An Experimental, Density Functional, and Correlated ab initio Study. *Chem. Eur. J.* **2005,** *11,* 204–224.

19. Gross, M. E.; Ibers, J. A.; Trogler, W. C. Structural and Spectroscopic Study of Cyclopentadienylcobalt N-Phenyl-o-benzoquinone Diimines. A Case for Delocalized T Bonding Organometallics. **1982**, *1*, 530–535.

20. (a) Miller, E. J.; Brill, T. B. The metal atom's view of the bonding in o-benzoquinone, o-dithiobenzoquinone, and o-benzoquinone diimine metallacycles of cyclopentadienylcobalt. A cobalt-59 NQR study of the cis-a3b2 ligand geometry. *Inorg. Chem.* **1983**, 22, 17, 2392-2398; (b) Miller, E. J.; Rheingold, A. L.; Brill, T. B. Bonding and structure in cyclopentadienylcobaltmetallacycle complexes. The crystal structures of [η^5-$C_5(CH_3)_5$]Co[$(NH)_2C_6H_4$] AND [η^5-$C_5(CH_3)_5$]Co[$(NH)SC_6H_4$]. *J. Organomet. Chem.* **1985**, 282, 399–412.

21. Alvarez, S. A cartography of the van der Waals territories. *Dalton Trans.* **2013**, *42*, 8617–8636.

22. Chelsea, M. R.; Iverson, B. L. Rethinking the Term "pi-stacking". Chem. Sci. **2012**, *3*, 2191–2201.

23. Macrae, C. F.; Bruno, I. J.; Chisholm, J. A.; Edgington, P. R.; McCabe, P.; Pidcock, E.; Rodriguez-Monge, L.; Taylor, R.; van de Streek, J.; Wood, P. A. Mercury CSD 2.0 - New Features for the Visualization and Investigation of Crystal Structures. *J. Appl. Cryst.* **2008**, *41*, 466–470.

24. D'Andrande, B. W.; Datta, S.; Forrest, R.; Djurovich, P.; Polikarpov, E.; Thompson, M. E. Relationship between the ionization and oxidation potentials of molecular organic semiconductors. *Org. Electron.* **2005**, *6*, 11–20.

25. Brédas, J. L.; Silbey, R.; Boudreaux, D. S.; Chance, R. R. Chain-Length Dependence of Electronica nd Electrochemical Properties of Conjugated Systems: Polyacetylene, Polyphenylene, Polythiophene, and Polypyrrole. *J. Am. Chem. Soc.* **1983**, *105*, 6555–6559.

26. (a) Becke, D. Density-functional thermochemistry. III. The role of exact exchange. *J. Chem. Phys.* **1993**, *98*, 5648–5652; (b) Lee, C.; Yang, W.; Parr, R. G. Development of the Colle-Salvetti correlation-energy formula into a functional of the electron density. *Phys. Rev. B* **1988**, *37*, 785–789.

27. Spackman, M. A.; Byrom P. G. A novel definition of a molecule in a crystal. *Chem. Phys. Lett.*, **1997**, *267*, 215–220.

28. Spackman, M. A.; Jayatilaka, D. Hirshfeld surface analysis *Cryst. Eng. Comm.* **2009**, *11*, 19–32.

29. McKinnon, J. J.; Spackman, M. A.; Mitchell, A. S. Novel tools for visualizing and exploring intermolecular interactions in molecular crystals. *Acta Cryst.* **2004**, *B60*, 627–668.

30. Spackman, M. A.; McKinnon, J. J. Fingerprinting intermolecular interactions in molecular crystals. *Cryst. Eng. Comm.* **2002**, *4*, 378–392.

31. McKinnon, J. J.; Jayatilaka, D.; Spackman, M. A. Towards quantitative analysis of intermolecular interactions with Hirshfeld surfaces. *Chem. Comm.* **2007**, 3814–3816.

32. http://www.flexcryst.com/html/home.pdf

33. Hofmann, D. W. M.; L. N. Kuleshova. Empirical temperature-dependent intermolecular potentials determined by data mining from crystal data. *Chem. Phys. Lett.* **2018**, 699, 115–124.

34. Hofmann, D. W. M. Data mining in organic crystallography. in *Data Mining in Crystallography*. Springer, Berlin, Heidelberg, 2009, 89–134.

35. King, R. B. Organometallic Chemistry of the Transition Metals. XI. Some New Cyclopentadienyl Derivatives of Cobalt and Rhodium. *Inorg. Chem.* **1966**, *5*, 82–87.

36. Heaton, A.; Hill, M.; Drakesmith, F. Polyhalogenonitrobenzenes and derived compounds Part 5. Improved preparations of 1,2,3,4-tetrafluoro-5,6-dinitrobenzene and 3,4,5,6-tetrafluoro-1,2-phenylenediamine, and the use of the latter for the synthesis of tetrafluorobenzheterocycles. *J. Fluorine Chem.* **1997**, *81*, 133–138.

37. Data Collection and Processing Software, Rigaku Corporation (1998-2015). Tokyo 196-8666, Japan.

38. Sheldrick, G. M. A short history of *SHELX*. *Acta Crystallogr.* **2008**, *A64*, 112–122.

39. Crystal Structure Analysis Package, Rigaku Corporation (2000-2017). Tokyo 196-8666, Japan.

40. Parr, R. G.; Yang, W. Density Functional Theory of Atoms and Molecules; Oxford University Press: Oxford, **1989**.

41. Frisch, M. J.; Trucks, G. W.; Schlegel, H. B.; Scuseria, G. E.; Robb, M. A.; Cheeseman, J. R.; Scalmani, G.; Barone, V.; Mennucci, B.; Petersson, G. A.; Nakatsuji, H.; Caricato, M.; Li, X.; Hratchian, H. P.; Izmaylov, A. F.; Bloino, J.; Zheng, G.; Sonnenberg, J. L.; Hada, M.; Ehara, M.; Toyota, K.; Fukuda, R.; Hasegawa, J.; Ishida, M.; Nakajima, T.; Honda, Y.; Kitao, O.; Nakai, H.; Vreven, T.; Montgomery, J. A., Jr.; Peralta, J. E.; Ogliaro, F.; Bearpark, M.; Heyd, J. J.; Brothers, E.; Kudin, K. N.; Staroverov, V. N.; Kobayashi, R.; Normand, J.; Raghavachari, K.; Rendell, A.; Burant, J. C.; Iyengar, S. S.; Tomasi, J.; Cossi, M.; Rega, N.; Millam, N. J.; Klene, M.; Knox, J. E.; Cross, J. B.; Bakken, V.; Adamo, C.; Jaramillo, J.; Gomperts, R.; Stratmann, R. E.; Yazyev, O.; Austin, A. J.; Cammi, R.; Pomelli, C.; Ochterski, J. W.; Martin, R. L.; Morokuma, K.; Zakrzewski, V. G.; Voth, G. A.; Salvador, P.; Dannenberg, J. J.; Dapprich, S.; Daniels, A. D.; Farkas, Ö.; Foresman, J. B.; Ortiz, J. V.; Cioslowski, J.; Fox, D. J. Gaussian 09 (Revision D.01), Gaussian, Inc., Wallingford CT, **2009**.

42. Perdew, J. P. Density-functional approximation for the correlation energy of the inhomogeneous electron gas. *Phys. Rev. B* **1986**, *33*, 8822–8824.

43. (a) Krishnan, R.; Binkley, J. S.; Seeger, R.; Pople, J. A. Self-consistent molecular orbital methods. XX. A basis set for correlated wave functions. *J. Chem. Phys.* **1980**, *72*, 650–654; (b) McLean, A. D.; Chandler, G. S. Contracted Gaussian basis sets for molecular calculations. I. Second row atoms, Z=11-18. *J. Chem. Phys.* **1980**, *72*, 5639–5648.

44. (a) Barone, V.; Cossi, M. Quantum Calculation of Molecular Energies and Energy Gradients in Solution by a Conductor Solvent Model. *J. Phys. Chem. A* **1998**, *102*, 1995–2001; (b) Cossi, M.; Rega, N.; Scalmani, G.; Barone, V. Energies, structures, and electronic properties of molecules in solution with the C-PCM solvation model. *J. Comp. Chem.* **2003**, *24*, 669–681.

45. Thompson, M. A. ArgusLab 4.0.1; Planaria Software LLC: Seattle, WA, http://www.arguslab.com/arguslab.com/ArgusLab.html/.

46. Espa, D.; Pilia, L.; Marchiò, L.; Mercuri, M. L.; Serpe, A.; Sessini, E.; Deplano, P. Near-infrared pigments based on ion-pair charge transfer salts of dicationic and dianionic metal-dithiolene [M(II) = Pd, Pt] complexes. *Dalton Trans.*, **2013**, *42*, 12429–12439. Crystal

47. CrystalExplorer (Version 3.1), Wolff, S. K.; Grimwood, D. J.; McKinnon, J. J.; Turner, M. J.; Jayatilaka, D.; Spackman, M. A.; University of Western Australia, **2012**.